CrystEngComm

Cite this: *CrystEngComm*, 2012, **14**, 370

www.rsc.org/crystengcomm

COMMUNICATION

Influence of CH_2Cl_2 for the structure stabilization of the Ni^{II} complex $[Ni\{6\text{-}MeO(O)CC_6H_4NHC(S)NP(S)(OiPr)_2\text{-}1,5\text{-}S,S'\}_2]\cdot CH_2Cl_2$†

Maria G. Babashkina,[a] Damir A. Safin,*[a] Monika Srebro,[b] Piotr Kubisiak,[b] Mariusz P. Mitoraj,[b] Michael Bolte[c] and Yann Garcia[a]

Received 5th October 2011, Accepted 10th November 2011
DOI: 10.1039/c1ce06322g

The reaction of the deprotonated *N*-thiophosphorylated thiourea 6-MeO(O)CC_6H_4NHC(S)NHP(S)$(OiPr)_2$ (HL) with $NiCl_2$ leads to violet $[NiL_2]\cdot CH_2Cl_2$ crystals, which were isolated by recrystallization from a mixture of CH_2Cl_2 and n-hexane. It was established that the deprotonated ligands, L, are 1,5-*S*,*S*′-coordinated. The influence of CH_2Cl_2 for the complex stabilization was studied.

Recently, it was demonstrated on a large number of examples that the deprotonated $R_2P(X)NHP(Y)R'_2$ (**PNP**) (X, Y = O, S, Se, Te)[1] and RC(S)NHC(X)R′ (**CNC**) (X = O, S)[2] are coordinated to the Ni^{II} cation through the donor X and Y atoms. This is, obviously, explained by the efficient delocalization of the negative charge in the symmetrical conjugated chelate backbone upon deprotonation. Contrariwise, the coordination mode of *N*-(thio)phosphorylated thioamides and thioureas $RC(S)NHP(X)(OR')_2$ (X = O, S) (**CNP**) towards Ni^{II} remains less studied. This is rather surprising since the negative charge is delocalized asymmetrically in the deprotonated **CNP** ligands and, hence, they might show ambidental coordination properties through the donor atoms of the thiocarbonyl and (thio) phosphoryl groups, and the nitrogen atom of the phosphorylamide group.[3] Furthermore, the nature of the R and R′ substituents might influence considerably the coordination mode of **CNP** both by the electronic and steric factors. Additional donor functions in these substituents might also affect crucially the complexation properties. Recently, we described the influence of the intramolecular H-bonding of the N–H···S=P type in **CNP** ligands (X = S) upon coordination to Ni^{II}.[4] We have also demonstrated solvent-induced coordination properties of *p*-$Me_2NC_6H_4NHC(S)NHP(S)(OiPr)_2$ towards Ni^{II}.[5] It was established that the arylNH hydrogen atoms are blocked through the formation of intermolecular hydrogen bonds with acetone molecules and, hence, 1,5-*S*,*S*′-coordination of the ligands towards Ni^{II} is realized. Thus, the nature of the solvent might influence considerably the stabilization of a certain isomer.

In this contribution, we describe the synthesis of **[NiL_2]**, a new Ni^{II} complex with the *N*-thiophosphorylated thiourea 6-MeO(O)CC_6H_4NHC(S)NHP(S)$(OiPr)_2$ (**HL**). Its molecular structure has been investigated in solution by multinuclear NMR and UV-vis absorption spectroscopy. Furthermore, the electronic properties of the isolated isomer were studied by cyclic voltammetry (CV). In order to characterize the electronic structure of **[NiL_2]** from a theoretical point of view, DFT based studies involving charge and energy decomposition bonding analysis (ETS-NOCV), ^{1}H NMR spectra and TD-DFT calculations were performed. The influence of the CH_2Cl_2 molecule, which is trapped during the crystallization, for the 1,5-*S*,*S*′-coordinated isomer stabilization was unequivocally established by DFT.

The **[NiL_2]** complex was prepared by deprotonating the ligand *in situ* using KOH, followed by reaction with $NiCl_2$ (Scheme 1, see also ESI†). The obtained dark violet solid material is soluble in most organic solvents and insoluble in n-hexane and water.

In the IR spectrum of **[NiL_2]** there is a band at 566 cm^{-1}, corresponding to the P=S group of the anionic forms **L**. The band is in the region characteristic of the 1,5-*S*,*S*′-coordinated complex forms.[3] There is also an intense band at 1528 cm^{-1}, corresponding to the conjugated SCN fragment, indicating complex formation.[3] In addition, there is a broad intense band arising from the POC group at 977 cm^{-1}. The spectrum contains the characteristic band for the

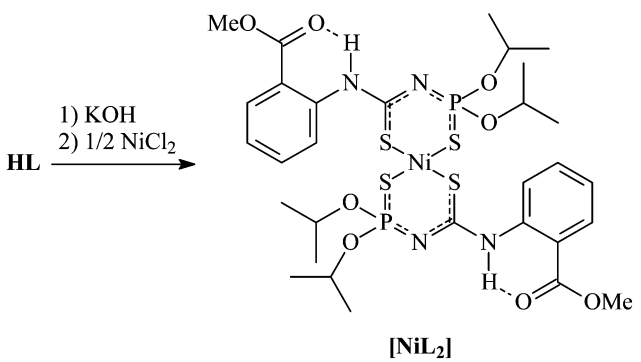

[NiL_2]

Scheme 1 Preparation of **[NiL_2]**.

[a]*Institute of Condensed Matter and Nanosciences, MOST - Inorganic Chemistry, Université Catholique de Louvain, Place L. Pasteur 1, 1348 Louvain-la-Neuve, Belgium. E-mail: damir.safin@ksu.ru; Fax: +32(0) 1047 2330; Tel: +32(0) 1047 2831*
[b]*Department of Theoretical Chemistry, Faculty of Chemistry, Jagiellonian University, R. Ingardena 3, 30-060 Cracow, Poland*
[c]*Institut für Anorganische Chemie J.-W.-Goethe-Universität, Frankfurt/Main, Germany*

† Electronic supplementary information (ESI) available: Additional data, Fig. S1 and S2, Tables S1–S3. CCDC reference number 805254. For ESI and crystallographic data in CIF or other electronic format see DOI: 10.1039/c1ce06322g

arylNH group at 3195 cm^{-1}. Furthermore, there is an intense band at 1690 cm^{-1}, corresponding to the C═O group.

The $^{31}P\{^1H\}$ NMR spectrum of **[NiL$_2$]** in $CDCl_3$ contains a unique singlet signal at 51.1 ppm, which indicates the exclusive presence of diamagnetic 1,5-*S*,*S*′-coordinated complex forms.[3–5] The ^1H NMR spectrum contains one set of signals. The signals of the isopropyl CH_3 protons are observed at 1.44–1.54 ppm, while the aryl CH_3 protons are at 3.92 ppm. The CHO protons are shown at 5.09 ppm. The signal for the NH protons shown at 11.21 ppm, which is in the low-field region, is due to the formation of intramolecular hydrogen bonds of the arylN–H···O═C type. The spectrum of the complex contains the signals of the phenylene rings at 6.99–8.57 ppm. As can be seen from Table 1, the calculated ^1H NMR chemical shifts for the **[NiL$_2$]·CH$_2$Cl$_2$** complex, based on GIAO approach[6] as implemented in the ADF package (version 2009.01[7]), are in a good agreement with the experimental results.

Dark violet **[NiL$_2$]·CH$_2$Cl$_2$** crystals were isolated by recrystallization from a 1 : 3 mixture of CH_2Cl_2 and n-hexane. The complex crystallizes in the triclinic space group $P\bar{1}$ (see ESI†). The metal is in a square planar *trans*-$S_2S'_2$ environment formed by the C═S and P═S sulfur atoms of two deprotonated ligands (Fig. 1). The six-membered NiSCNPS metallocycles have an asymmetric boat form. The values of the intracyclic S–Ni–S angles are about 99° (Table S1 in ESI†). The lengthening of the C═S and shortening of the C–N bonds are observed upon complex formation compared to **NTT** ligands.[3–5] The same change, but to a smaller degree, has been observed for the P–N and P═S bonds. The arylNH protons are involved in intramolecular hydrogen bonds of the N–H···O═C type (Fig. 1, Table S2 in ESI†). Due to these intramolecular hydrogen bonds the NH hydrogen atoms are blocked and, hence, are not suitable for the formation of the intramolecular H-bonding of the N–H···S═P type, allowing the 1,3-*N*,*S*-coordination mode of the ligand towards Ni^{II}.[4,5] Furthermore, there are two intermolecular hydrogen bonds of the C–H···O═C and C–H···S═C type, which are formed between the oxygen atom of the carbonyl group and the sulfur atom of the thiocarbonyl group, respectively, and the hydrogen atoms of the dichloromethane molecule, which is trapped during the crystallization (Fig. 1, Table S2 in ESI†)

To examine the intermolecular C–H···O═C and C–H···S═C interactions in the complex **[NiL$_2$]·CH$_2$Cl$_2$**, a recently proposed charge and energy decomposition scheme ETS-NOCV[8] was applied based on the ADF program.[7] Details on the original energy decomposition method ETS and combined ETS-NOCV scheme can be found in ESI†. The geometry of the **[NiL$_2$]·CH$_2$Cl$_2$** complex has been optimized at the B3LYP level of theory, as implemented in the Gaussian 09 package.[9] The main advantage of the ETS-NOCV scheme is that it provides both a qualitative and quantitative picture of chemical bond formation within one common theoretical framework.

Table 1 Calculated and experimental ^1H NMR chemical shifts in ppm (values relative to $SiMe_4$) for **[NiL$_2$]·CH$_2$Cl$_2$**

	Calculated	Experimental
CH_3 (*i*Pr)	1.54	1.44–1.54
CH_3 (aryl)	3.98	3.92
OCH (*i*Pr)	6.71	5.09
CH (aryl)	8.07	6.99–8.57
NH	12.69	11.21

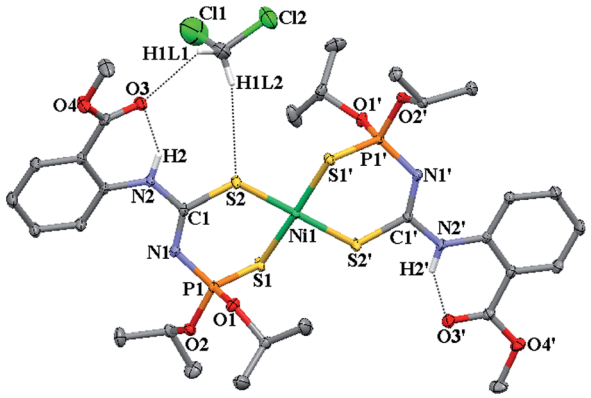

Fig. 1 Thermal ellipsoid (30%) plot of **[NiL$_2$]·CH$_2$Cl$_2$**. H-atoms, not involved in hydrogen bonding, were omitted for clarity.

The qualitative picture of bonding originates from the depiction of deformation density contributions ($\Delta\rho_i$) that characterize the formation of specific bonding channels (σ, π, *etc.*). In the ETS-NOCV scheme the quantitative picture of bonding is obtained by providing the energies [ΔE_{orb}(i)] associated with each charge flow-channel ($\Delta\rho_i$). It was shown that ETS-NOCV is especially useful when describing bonding between molecular fragments.[8] Therefore, we described the bonding between CH_2Cl_2 and the rest of the complex (see black circle line in Fig. 2) using the dispersion corrected BP86-D functional with TZ2P basis set for all elements.[7] It can clearly be seen from Fig. 2 (panel **A**) that the total interaction energy, $\Delta E_{total} = -7.2$ kcal mol^{-1}, between CH_2Cl_2 and **[NiL$_2$]**, is dominated by the electrostatic factor ($\Delta E_{elstat} = -6.8$ kcal mol^{-1}). This can be related to the stabilization arising from the following interactions

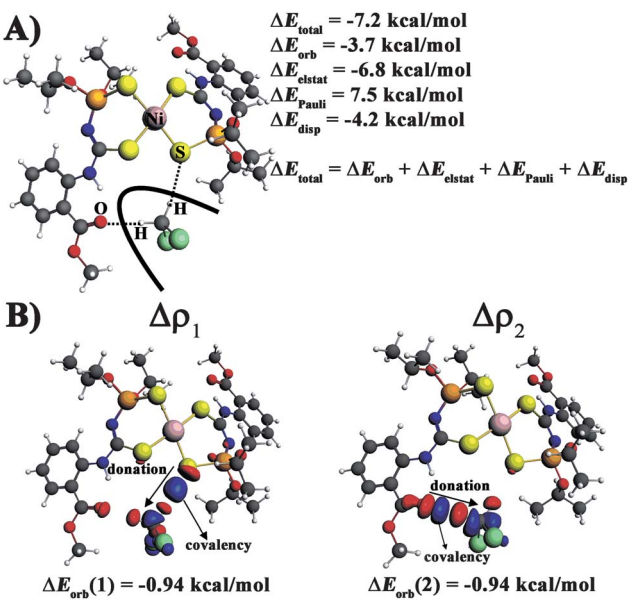

Fig. 2 ETS energy decomposition results, characterizing the interaction between **CH$_2$Cl$_2$** and **[NiL$_2$]**, are presented in panel **A**, whereas the deformation densities $\Delta\rho_i$ and the corresponding energies ΔE_{orb}(i), originating from the ETS-NOCV scheme, are shown in panel **B**. Red color of $\Delta\rho_i$ exhibits charge depletion, whereas blue color exhibits charge accumulation upon bond formation.

$CH^{\delta+}$–$O^{\delta'-}$ and $CH^{\delta+}$–$S^{\delta'-}$. A very important contribution originates from the dispersion stabilization – the estimated value is $\Delta E_{disp} = -4.2$ kcal mol^{-1}. Electronic stabilization due to the charge rearrangment upon hydrogen bond formation is slightly less important and amounts to $\Delta E_{orb} = -3.7$ kcal mol^{-1}. It is gratifying to see that the two deformation density channels, $\Delta\rho_1$ and $\Delta\rho_2$ based on NOCV's, characterize separately the formation of C–H···O═C and C–H···S═C bonds (Fig. 2, **B**). Qualitatively these bonds are characterized by the charge donation from the lone electron pair of oxygen (in the case of C–H···O═C) and sulfur (for C–H···S═C) into the empty σ*(C–H) orbitals of CH_2Cl_2. In addition, an evident covalent component is formed, *i.e.* the shift of electron density from hydrogen atoms of CH_2Cl_2 and the electron donors (O or S) into the bonding regions of C–H···O═C and C–H···S═C is observed (Fig. 2, **B**). The presence of a covalent component in hydrogen bonded systems has been recently highlighted by Grabowski.[10] Quantitatively, both types of intermolecular interaction have the same strength (−0.94 kcal mol^{-1}).

It is noteworthy that we have also calculated the 1,3-*N*,*S*- and non-solvated 1,5-*S*,*S*′-conformations of the **[NiL$_2$]** complex. Comparing the energies between these isomers one might notice higher (by 3.6 kcal mol^{-1}) stabilization in the case of the 1,3-*N*,*S*-structure. ETS-NOCV indicated that it can be related to the presence of the intramolecular N–H···O═C and N–H···S═P interactions as well as stronger amine bonding (Fig. S1 and S2 and Table S1 in ESI†). Clearly, when including an extra stabilization due to the hydrogen bond formation by the CH_2Cl_2 molecule, the 1,5-*S*,*S*′-conformation of **[NiL$_2$]·CH$_2$Cl$_2$** becomes more stable (by 3.6 kcal mol^{-1}) as compared to the 1,3-*N*,*S*-conformation (Fig. S1 in ESI†). It is in line with the experimental results indicating that in a CH_2Cl_2 solution, the 1,5-*S*,*S*′-conformation is predominantly observed.

Dissolving the complex **[NiL$_2$]** in CH_2Cl_2 leads to a greenish-blue solution. The UV-vis absorption spectrum contains two UV bands at 254 and around 270 nm. These bands can be assigned to corresponding intraligand transitions (π–π* or n–π* type).[4b,5] The visible region of the spectrum contains two absorption bands at 537 and about 660 nm. From the rather low intensities (179–188 M^{-1} cm^{-1}) of the two long-wavelength bands, they are assigned to ligand field (d–d) transitions. Thus, the assumption that the complex is exclusively 1,5-*S*,*S*′ configured in solution is strongly supported by the absorption spectrum.

The electrochemistry of the complex **[NiL$_2$]** was measured using cyclic voltammetry (Table 2). A reversible first one-electron reduction at −1.47 V is caused by a ligand-centred reduction.[4b,5] On the oxidative side, the first wave occurs at +0.39 V followed by a second one at +0.73 V. The oxidation is attributed also to a ligand-centred process since the observed vast difference in oxidation potentials is too large to be attributed to a nickel-centred oxidation Ni^{II}/Ni^{III}. The assumption of a ligand-based oxidation is also in line with the absorption spectroscopy, which gave no evidence for a metal-to-ligand or ligand-to-metal charge transfer.

Table 2 Selected electrochemical data for **[NiL$_2$]** in CH_2Cl_2[a]

E_{pa} (Ox 3)	E_{pa} (Ox 2)	E_{pa} (Ox 1)	E_{pa} (Red 1)	E_{pc} (Red 1)	$E_{1/2}$ (Red 1)
0.73	0.39	−0.02	−1.38	−1.47	−1.43

[a] From cyclic voltammetry in 0.1 M nBu$_4$NPF$_6$/solvent solutions at 100 mV s^{-1} scan rate. Potentials in V *vs.* FeCp$_2^{+/0}$. Half-wave potentials $E_{1/2}$ for reversible processes, peak potential differences $\Delta E_{pp} = E_{pa} - E_{pc}$ in mV in parentheses (the value for ferrocene was 68 mV), cathodic peak potentials E_{pc} and anodic peak potentials E_{pa}.

In order to gain further qualitative insight into the nature of the absorption spectrum for the **[NiL$_2$]·CH$_2$Cl$_2$** complex, the time dependent density functional method was applied (TD-DFT) as implemented in Gaussian package.[9] The simulated spectrum (at the DFT/B3LYP level of theory) in the gas phase together with the selected molecular orbitals involved in the dominant transitions are presented in Fig. 3. The absorption spectrum plot was obtained using the Swizard software,[11] whereas contours of molecular orbitals were generated by the GaussView program.[12]

It can clearly be seen from Fig. 3 (part **A**) that one dominant band, with the largest oscillator strength $f = 0.2830$ a.u. was obtained at 388 nm. This transition is dominated by HOMO−5 → LUMO and HOMO → LUMO+1 charge transfers. It can be noticed qualitatively (Fig. 3, **B**) that the former one characterizes predominantly

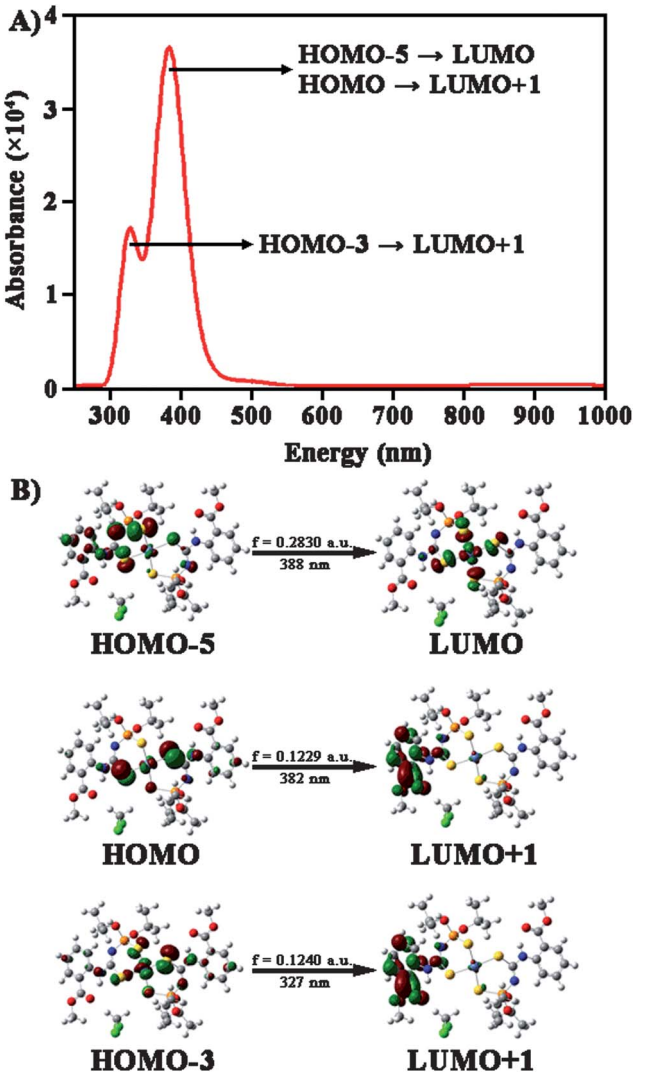

Fig. 3 The simulated TD-DFT/B3LYP spectrum of **[NiL$_2$]·CH$_2$Cl$_2$** in the gas phase (part **A**) together with the contours of molecular orbitals (0.04 a.u.) involved in the dominant transitions (part **B**).

intra-ligand charge transfer from the π-type orbital of the aryl ring and the lone electron pairs of sulfur (HOMO−5) and the charge accumulation into the anti-bonding Ni–S orbitals (predominantly σ*). A ligand to metal charge transfer (LMCT) contribution is also visible. Minor participation of the d–d charge transfer can be noted from the presented contours. The latter transfer (HOMO → LUMO+1) with $f = 0.1229$ a.u., which also contributes to the most dominant band, involves mostly the outflow of electron density from lone electron pairs of sulfur into the empty π* orbital of the aryl ring. Finally, a far less intense peak ($f = 0.1240$ a.u.) was found at 327 nm, assigned to the HOMO−3 → LUMO+1 transition. It corresponds predominantly to intra-ligand charge transfer (ILCT), although some contribution originating from the metal to ligand charge transfer (MLCT) is also clearly visible (see HOMO−3 and LUMO+1 contours).

Evident domination of the intra-ligand oxidation is thus in line with the experimental findings based on CV experiments.

To conclude, we have synthesized a Ni^{II} complex with *N*-thiophosphorylatedthiourea 6-MeO(O)CC_6H_4NHC(S)NHP(S)(O*i*Pr)$_2$ (**HL**). According to the NMR, UV-vis, IR and X-ray analysis data the complex **[NiL$_2$]** was found to be exclusively dithiocoordinated both in solution and in the solid state. The DFT based ^{1}H HMR results for the dithiocoordinated complex **[NiL$_2$]** appeared to be in a very good agreement with the experimental data. The charge and energy decomposition scheme (ETS-NOCV) deeply characterized the bonding and stability of **[NiL$_2$]**. Finally, the TD-DFT study has indicated that the absorption spectrum is dominated by the intra-ligand transition, which is in line with the CV experiments. Furthermore, according to the DFT data the crucial role of a CH_2Cl_2 molecule, which is trapped during the crystallization and is bound to the **[NiL$_2$]** complex through intermolecular hydrogen bonds C–H···O=C and C–H···S=C, for the 1,5-*S*,*S*′-coordinated isomer stabilization was established.

Acknowledgements

M. P. Mitoraj greatly acknowledges the financial supports from Polish Ministry of Science and Higher Education ("Outstanding Young Researchers" scholarship). M. Srebro also acknowledges the financial support from the Foundation for Polish Science ("START" scholarship). We are also grateful to ACK CYFRONET – Krakow, to the Laboratory of Parallel Computing of the Institute of Computer Science AGH for the computer time and to the F.R.S.-FNRS (Belgium) for financial support as well as a post-doctoral position to D. A. Safin.

Notes and references

1 For examples (*a*) I. Haiduc, *J. Organomet. Chem.*, 2001, **623**, 29; (*b*) I. Haiduc, Inorganic (carbon-free) chelate rings: a dithioimidodiphosphinato ligand and some of its metal complexes, in *Inorganic Experiments* (3rd Edition), ed. J. D. Woollins, 2010, Wiley-VCH Verlag GmbH&Co. KGaA, Weinheim, Germany, p. 229.
2 For examples (*a*) K. R. Koch, O. Hallale, S. A. Bourne, J. Miller and J. Bacsa, *J. Mol. Struct.*, 2001, **561**, 185; (*b*) S. A. Bourne, O. Hallale and K. R. Koch, *Cryst. Growth Des.*, 2005, **5**, 307; (*c*) O. Hallale, S. A. Bourne and K. R. Koch, *New J. Chem.*, 2005, **29**, 1416; (*d*) O. Hallale, S. A. Bourne and K. R. Koch, *CrystEngComm*, 2005, **7**, 161.
3 (*a*) F. D. Sokolov, V. V. Brusko, N. G. Zabirov and R. A. Cherkasov, *Curr. Org. Chem.*, 2006, **10**, 27; (*b*) F. D. Sokolov, V. V. Brusko, D. A. Safin, R. A. Cherkasov and N. G. Zabirov, Coordination Diversity of *N*-Phosphorylated Amides and Ureas Towards VIIIB Group Cations, in *Transition Metal Chemistry: New Research*, ed. B. Varga and L. Kis, 2008, Nova Science Publishers Inc., Hauppauge NY, USA, p. 101 and references therein.
4 (*a*) M. G. Babashkina, D. A. Safin, M. Bolte and A. Klein, *Inorg. Chem. Commun.*, 2009, **12**, 678; (*b*) M. G. Babashkina, D. A. Safin, M. Bolte, M. Srebro, M. Mitoraj, A. Uthe, A. Klein and M. Köckerling, *Dalton Trans.*, 2011, **40**, 3142.
5 M. G. Babashkina, D. A. Safin, M. Srebro, P. Kubisiak, M. Mitoraj, M. Bolte and Y. Garcia, *CrystEngComm*, 2011, **13**, 5321.
6 G. Schreckenbach and T. Ziegler, *J. Phys. Chem.*, 1995, **99**, 606.
7 (*a*) G. te Velde, F. M. Bickelhaupt, E. J. Baerends, C. Fonseca Guerra, S. J. A. van Gisbergen, J. G. Snijders and T. Ziegler, *J. Comput. Chem.*, 2001, **22**, 931, and references therein; (*b*) E. J. Baerends, J. Autschbach, D. Bashford, A. Bérces, F. M. Bickelhaupt, C. Bo, P. M. Boerrigter, L. Cavallo, D. P. Chong, L. Deng, R. M. Dickson, D. E. Ellis, M. van Faassen, L. Fan, T. H. Fischer, C. Fonseca Guerra, A. Ghysels, A. Giammona, S. J. A. van Gisbergen, A. W. Götz, J. A. Groeneveld, O. V. Gritsenko, M. Grüning, F. E. Harris, P. van den Hoek, C. R. Jacob, H. Jacobsen, L. Jensen, G. van Kessel, F. Kootstra, M. V. Krykunov, E. van Lenthe, D. A. McCormack, A. Michalak, M. Mitoraj, J. Neugebauer, V. P. Nicu, L. Noodleman, V. P. Osinga, S. Patchkovskii, P. H. T. Philipsen, D. Post, C. C. Pye, W. Ravenek, J. I. Rodríguez, P. Ros, P. R. T. Schipper, G. Schreckenbach, M. Seth, J. G. Snijders, M. Solà, M. Swart, D. Swerhone, G. te Velde, P. Vernooijs, L. Versluis, L. Visscher, O. Visser, F. Wang, T. A. Wesolowski, E. M. van Wezenbeek, G. Wiesenekker, S. K. Wolff, T. K. Woo, A. L. Yakovlev and T. Ziegler, *Theoretical Chemistry*, Vrije Universiteit, Amsterdam.
8 M. Mitoraj, A. Michalak and T. Ziegler, *J. Chem. Theory Comput.*, 2009, **5**, 962.
9 M. J. Frisch, G. W. Trucks, H. B. Schlegel, G. E. Scuseria, M. A. Robb, J. R. Cheeseman, G. Scalmani, V. Barone, B. Mennucci, G. A. Petersson, H. Nakatsuji, M. Caricato, X. Li, H. P. Hratchian, A. F. Izmaylov, J. Bloino, G. Zheng, J. L. Sonnenberg, M. Hada, M. Ehara, K. Toyota, R. Fukuda, J. Hasegawa, M. Ishida, T. Nakajima, Y. Honda, O. Kitao, H. Nakai, T. Vreven, J. A. Montgomery Jr., J. E. Peralta, F. Ogliaro, M. Bearpark, J. J. Heyd, E. Brothers, K. N. Kudin, V. N. Staroverov, R. Kobayashi, J. Normand, K. Raghavachari, A. Rendell, J. C. Burant, S. S. Iyengar, J. Tomasi, M. Cossi, N. Rega, J. M. Millam, M. Klene, J. E. Knox, J. B. Cross, V. Bakken, C. Adamo, J. Jaramillo, R. Gomperts, R. E. Stratmann, O. Yazyev, A. J. Austin, R. Cammi, C. Pomelli, J. W. Ochterski, R. L. Martin, K. Morokuma, V. G. Zakrzewski, G. A. Voth, P. Salvador, J. J. Dannenberg, S. Dapprich, A. D. Daniels, Ö. Farkas, J. B. Foresman, J. V. Ortiz, J. Cioslowski and D. J. Fox, *Gaussian 09*, Gaussian Inc., Wallingford CT, 2009.
10 S. Grabowski, *Chem. Rev.*, 2011, **111**, 2597.
11 (*a*) S. I. Gorelsky *SWizard program*, http://www.sg-chem.net/, University of Ottawa, Ottawa, Canada, 2010; (*b*) S. I. Gorelsky and A. B. P. Lever, *J. Organomet. Chem.*, 2001, **635**, 187.
12 R. Dennington, T. Keith and J. Millam, *Semichem Inc.*, Shawnee Mission KS, 2009.